COMMUNICATION

Check for updates

Microsecond charge separation at heterojunctions between transition metal dichalcogenide monolayers and single-walled carbon nanotubes†

Dana B. Sulas-Kern, [ID] Hanyu Zhang, [ID] Zhaodong Li and Jeffrey L. Blackburn [ID] *

The use of monolayer transition metal dichalcogenides (TMDCs) for optical-to-electrical or optical-to-chemical energy conversion can be limited by the ultrafast excited state relaxation inherent to neat monolayers. Photoinduced charge separation at nanoscale heterojunctions is an important strategy to extend carrier lifetimes, enabling photodetectors, solar cells, and solar fuel production with these ultrathin materials. We demonstrate TMDC/single-walled carbon nanotube (SWCNT) heterojunctions with exceptionally long, microsecond timescale, charge separation following sub-picosecond interfacial charge transfer. These carrier lifetimes are orders of magnitude longer-lived than in other monolayer TMDC heterojunctions. We further present two unique methodologies for estimating charge-transfer quantum yields in MoS_2 that can be broadly applied and refined for other TMDC systems. Our results highlight the promise of TMDC/SWCNT heterojunctions for advanced (photo)catalytic and optoelectronic systems and devices.

New concepts

Long-lived separated charge carriers are a prerequisite for efficiently converting photon energy to electricity or fuels in solar energy harvesting devices. Here, we counteract ultrafast excited state decay in transition metal dichalcogenide (TMDC) monolayers by demonstrating that heterojunctions between MoS_2 and single-walled carbon nanotubes enable remarkably long carrier lifetimes in the microsecond time range. The photoexcited free charges in this system differ from the Coulomb-bound interfacial states found in several other TMDC heterojunctions, and the long lifetimes in this case may enable facile current extraction and complex multi-electron photocatalytic reactions, opening avenues for efficient photocurrent generation and hydrogen evolution. With a goal of enabling systematic investigations of charge separation in TMDCs and their heterojunctions, we introduce broadly applicable concepts for quantifying practical metrics necessary for high-efficiency devices (*e.g.* carrier lifetimes, yields, and generation rates) and for analysing the fundamental mechanisms underlying charge separation.

Introduction

Two-dimensional (2D) transition metal dichalcogenides (TMDCs) have received recent attention for their promise in catalytic,[1–3] logic,[6] semiconducting,[7–9] and optoelectronic devices.[10–13] Although initial discovery of TMDCs dates back to 1923[15] and monolayers were achieved in 1986,[16] the advances necessary to harness the exceptional properties of TMDC monolayers came much later with graphene-related development in the early 2000's,[17] spurring a rapid increase in TMDC interest over the past five years.[18,19] Unlike graphene, many TMDCs have a natural band gap in the visible range, enabling light-harvesting applications with a similarly ultrathin material. The synergy between confined spatial structure and the unique TMDC energy landscape (for example, including a spin–orbit split valence band and a transition from indirect to direct band gap at the monolayer limit[20,21]) introduces a vast array of technologically valuable phenomena such as chemical and mechanical tunability of the band structure and excited state populations,[22–25] spin-valley locking,[26,27] quantum confinement,[21,28,29] high absorption coefficients,[10] excellent thickness-normalized device metrics,[10,12] large magneto-resistance,[30,31] and superconductivity.[18,31,32]

Despite the great promise and rich (photo)physics in TMDCs, the performance of TMDC devices that rely on efficient photo-current generation can be limited by large exciton binding energies[5,33,34] and the resulting ultrafast excited state decay that is often observed on picosecond time scales.[35] For example, while TMDCs such as MoS_2 show promise as stable, earth-abundant, and cost-effective (photo)catalysts for hydrogen fuel production, high photocatalytic activity depends upon achieving sufficiently long carrier lifetimes for electron diffusion to active sites and subsequent transfer from the TMDC to adsorbed hydrogen.[3] Similarly, in photovoltaic applications, fast recombination in competition with charge extraction is likely an important factor causing sub-unity internal quantum efficiencies and low

National Renewable Energy Laboratory, Golden, Colorado 80401, USA.
E-mail: Jeffrey.blackburn@nrel.gov

open-circuit voltages.[12,13] To realize the long carrier lifetimes necessary for functional TMDC applications, several hybrid structures are actively being investigated (*e.g.* stacked TMDC/TMDC,[13,36,37] lateral multilayer–monolayer TMDC,[38–40] TMDC/graphene,[6] TMDC/organic,[12,41–44] TMDC/quantum dots,[45] TMDC/Si,[46] TMDC/carbon nitride[47]), where charge transfer across a heterojunction combats recombination and extends excited state lifetimes through exciton dissociation and spatial separation of electrons from holes.

While charge carrier lifetimes have been extended up to nanosecond time scales in some of these TMDC heterojunctions,[42,44] in this study we demonstrate orders of magnitude longer-lived kinetics with carriers persisting past 1 μs in Type-II heterojunctions of monolayer MoS_2 with (6,5) semiconducting single-walled carbon nanotube (SWCNT) films. The pairing of MoS_2 with SWCNTs is particularly appealing due to the diameter-dependent tunability of the SWCNT energy landscape,[48] the high photochemical stability of SWCNTs,[49] and previous demonstrations of SWCNTs sustaining long-lived charge in other donor/acceptor heterojunctions.[14,50,51] Encouragingly, both photocurrent and hydrogen evolution have been observed in a few TMDC/SWCNT systems, although these systems most often contain mixed SWCNTs with a broad range of electronic structure and amorphous or multilayer TMDCs.[2,49,52,53]

Because the fundamental photophysical processes at monolayer TMDC/SWCNT heterojunctions have been largely unexplored, we present a detailed model of the ultrafast charge-transfer process leading to exceptionally long-lived separated charges.

By fitting our transient absorption (TA) data using a global target analysis based on singular value decomposition,[54] we quantify sub-picosecond charge generation, including both electron transfer to MoS_2 following selective SWCNT excitation ($\tau_{ET} \approx 0.8$ ps) and hole transfer to the SWCNT layer following selective MoS_2 excitation ($\tau_{HT} \approx 0.5$ ps). We evaluate charge-transfer yields based on the empirically-determined SWCNT absorption cross section,[50] and we further discuss the charge-transfer yields in the context of a phase-space filling model that relates the magnitude of MoS_2 carrier-induced exciton quenching to the MoS_2 dielectric constant and exciton mass. Our study highlights the promise of pairing SWCNTs with TMDC monolayers both for sustaining remarkably long-lived charge carriers in photocatalytic and optoelectronic applications and for use as clean model systems with easily distinguishable and quantifiable spectral signatures for optical studies.

Experimental results

MoS_2/SWCNT heterojunctions

Fig. 1A depicts the energy level offsets at the monolayer MoS_2/(6,5)SWCNT interface, showing that this system is expected to form a Type-II heterojunction. In Fig. 1B, we illustrate that charge transfer generates negative charge on MoS_2 after photoexcitation of either layer (process 1), after which efficient charge transport and delocalization within the SWCNT layer[55,56] likely serves an essential role to prevent recombination at the interface
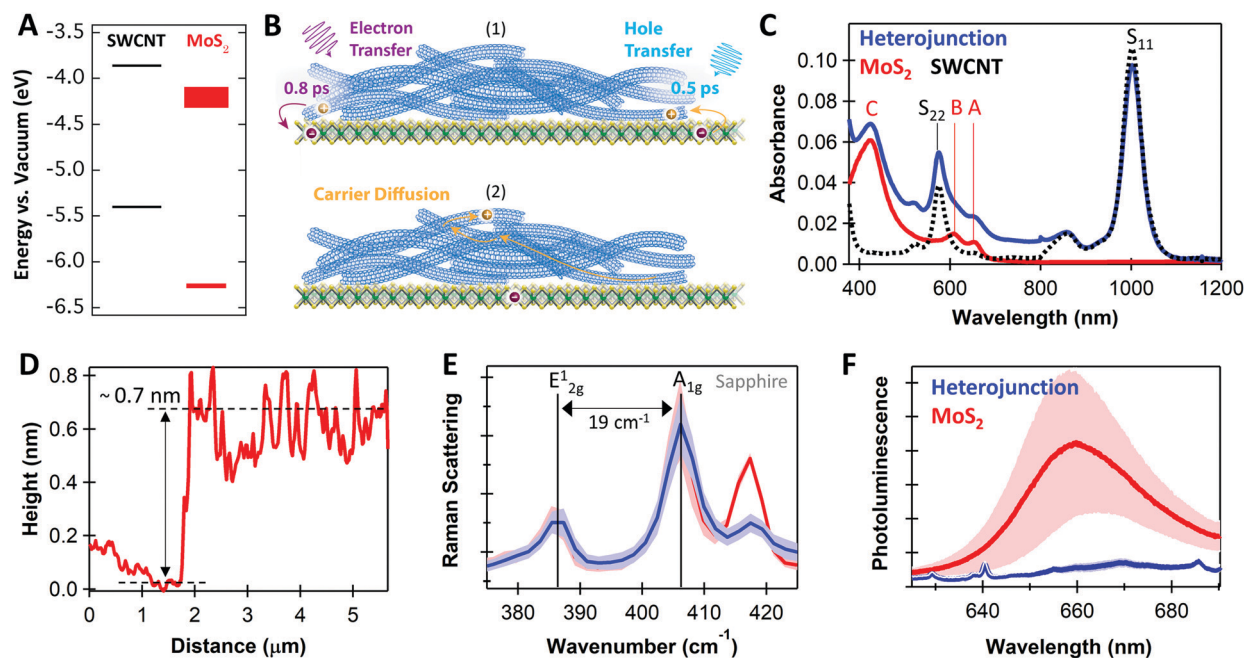
Fig. 1 (A) Energy level diagram for monolayer MoS_2 and (6,5)SWCNTs with values from ref. 5 and 14; (B) schematic of (1) photoexcited charge transfer and (2) carrier diffusion, with time constants from our transient absorption analysis; (C) absorbance spectra for neat MoS_2 (red), neat SWCNT (black dotted), and MoS_2/SWCNT heterojunctions (blue); (D) atomic force microscopy height profile across a scratch for the neat MoS_2 monolayer; (E) Raman scattering for neat MoS_2 (red) and the heterojunction (blue); (F) photoluminescence spectra for MoS_2 (red) and MoS_2/SWCNT heterojunctions (blue), where sharp peaks in the heterojunction spectrum are SWCNT Raman modes. Shading in (E and F) represents the standard deviation of the mean for 15 measurements with 532 nm excitation, which likely arises from variations in local chemical environment and substrate interactions.

by supporting spatial carrier separation (process 2). As our schematic implies, the ultrathin nature of MoS_2 monolayers limit the vertical distance that electrons can move away from the interface, suggesting that hole transport in the SWCNT layer may be crucial for sustaining long-lived charge.

The thermodynamic driving force for free carrier generation depends on the energetic difference between initially photo-excited excitons and the final separated charges. We estimate the driving force as $\Delta G_{ET/HT} = (IP_D - EA_A) - E_{opt,D/opt,A}$, where $\Delta G_{ET/HT}$ is the change in free energy following electron transfer (ET) or hole transfer (HT), IP_D and $E_{opt,D}$ are the ionization potential and optical gap of the SWCNT donor, and EA_A and $E_{opt,A}$ are the electron affinity and optical gap of the MoS_2 acceptor.[57] Using the energies in Fig. 1A, we estimate that MoS_2 exciton dissociation followed by hole transfer to the SWCNTs is favorable by −620 meV. Calculating ΔG_{ET} has more significant uncertainty due to greater variation of the MoS_2 electron affinity in the literature. Using reported values of EA_{MoS_2} of −4.15 to −4.25 eV,[5] we estimate ΔG_{ET} in the range of −90 to +10 meV. We note that MoS_2 excitation can also result in excitation energy transfer (EET) from MoS_2 to SWCNTs due to the larger bandgap of MoS_2.

As shown in Fig. 1C, the complementary absorbance peaks of MoS_2 and (6,5)SWCNTs make this an ideal model system for optical studies of excited-state dynamics at TMDC hetero-junctions. The S_{11} absorption at 1000 nm allows selective photoexcitation of low-energy SWCNT excitons. Subsequently, charge transfer is the only pathway for moving a carrier population onto MoS_2, because the 1000 nm photons are too low in energy for direct MoS_2 excitation and EET from SWCNTs to MoS_2 is significantly uphill in energy. Additionally, the MoS_2 C exciton absorption at 440 nm peaks at an absorption minimum for the SWCNTs, allowing selective probing of hole transfer from MoS_2 to the SWCNTs. Furthermore, the MoS_2 A (660 nm) and B (610 nm) exciton peaks show minimal overlap with the SWCNT S_{22} absorption, allowing us to clearly track MoS_2 bleaching during TA analysis. This clean spectral separation contrasts with previous heterojunction studies where overlapping absorption spectra must be carefully considered to evaluate charge separation mechanisms from optical studies.[42,44]

Fig. 1D–F demonstrate that the MoS_2 used in our studies are indeed monolayers. The ∼0.7 nm atomic force microscopy (AFM) height profile (Fig. 1D), the 19 cm^{-1} energy difference between in-plane (E^1_{2g}) and out-of-plane (A_{1g}) Raman peaks (Fig. 1E), and the 660 nm photoluminescence (PL) peak position (Fig. 1F) are all characteristic of monolayers.[25,58]

Long-lived photoinduced charge formation

In Fig. 1F, the MoS_2 PL is strongly quenched in the MoS_2/SWCNT heterojunction compared to the neat monolayer, suggesting that photoinduced charge transfer likely occurs across the heterojunction. However, PL quenching cannot discern between charge and energy transfer, as both processes deplete emissive MoS_2 excitons. Thus, we use transient absorption (TA) spectroscopy to quantify charge transfer at MoS_2/SWCNT interfaces. We show that separated carriers form with sub-picosecond

kinetics following selective photoexcitation of either the MoS_2 or the SWCNT layers and that charge separation persists up to the microsecond timescale.

Fig. 2A and C show the long-lived TA spectra that persist in the heterojunction following both 440 and 1000 nm excitation. With either excitation wavelength, the NIR signal in the hetero-junction is enhanced compared to the neat materials. The NIR peaks are signatures of a SWCNT charge carrier population, including the trion induced absorption at 1175 nm and bleaching of the S_{11} transition at 1000 nm.[50] The SWCNT charge signatures in the heterojunction indicate that both processes are thermo-dynamically and kinetically accessible, including photoinduced hole transfer from excited MoS_2 to the SWCNT layer (Fig. 2A, 440 nm excitation) and electron transfer from SWCNTs to MoS_2 (Fig. 2C, 1000 nm excitation).

In the visible range, we attribute bleaching at 610 nm and 650 nm to the MoS_2 A and B excitons, respectively, and we attribute the 575 nm bleach to the SWCNT S_{22} transition. We observe MoS_2 bleaching even with low-energy 1000 nm excita-tion, indicating that electron transfer from the SWCNTs to MoS_2 must take place. The 440 nm excitation generates similar MoS_2 bleach magnitude in both the heterojunction and neat monolayer. We note that the unchanged MoS_2 bleach ampli-tude in this case does suggest that a greater electron density is sustained on MoS_2 with the heterojunction. This is because the bleach in neat MoS_2 is either due to excitons or a mix of spontaneously separated electrons and holes, while the bleach in the heterojunction is primarily due to only electrons after the holes are donated to the SWCNTs. The demonstration of both photoinduced hole transfer from MoS_2 to SWCNT and electron transfer from SWCNT to MoS_2 is consistent with the Type-II energetic alignment and thermodynamic driving forces proposed in Fig. 1A.

In Fig. 2B and D, we show the charge-related kinetics at the SWCNT trion induced absorption at 1175 nm, demonstrating longer-lived carrier kinetics in the heterojunctions compared to the neat SWCNTs. Importantly, the charge-associated signal in the heterojunction does not fully decay within the 5 ns delay window regardless of the excitation wavelength. We note that the heterojunction kinetics with 1000 nm excitation in Fig. 2D show an initial fast decay component corresponding to SWCNT excitons that have non-negligible contribution to the signal at 1175 nm (further discussed in Fig. 4A). The SWCNT excitons either decay to the ground state or undergo charge separation, and longer-lived carrier kinetics similar to the 440 nm excita-tion dominate at later times.

Fig. 3 shows that the separated charge carriers persist up to the microsecond time scale in the monolayer MoS_2/SWCNT hetero-junction, and that the kinetics on these longer time scales are similar for selective excitation of either MoS_2 or the SWCNT layer. Recombination on long timescales follows a multiexponential decay with an amplitude-averaged lifetime of 0.73 μs from components of 17.5 ns (43%), 233 ns (43%), and 4.4 μs (14%). These kinetics demonstrate the longest carrier lifetimes to our knowledge in monolayer TMDC heterojunctions that have been measured with TA spectroscopy at room temperature.

Fig. 2 (A) Transient absorption spectra averaged over 2–5 ns following 440 nm excitation of neat MoS_2 (red), neat SWCNT (black dotted), and MoS_2/SWCNT heterojunctions (blue); (B) kinetic traces at 1175 nm, corresponding to the SWCNT trion (X^+) induced absorption with 440 nm excitation; (C) transient absorption spectra averaged over 2–5 ns following 1000 nm excitation; (D) kinetic traces at the SWCNT trion induced absorption with 1000 nm excitation.
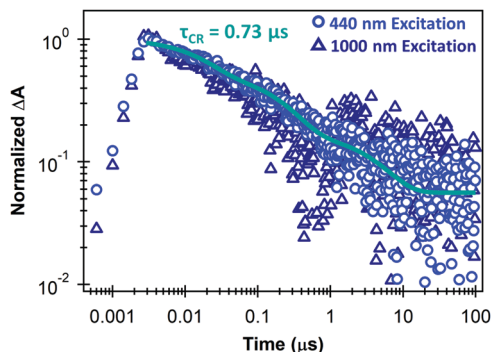

Fig. 3 Carrier kinetics at 1175 nm (trion induced absorption) on the microsecond time scale for monolayer MoS_2/SWCNT heterojunctions under 440 nm excitation (light blue circles) or 1000 nm excitation (dark blue triangles), showing a triexponential fit with an amplitude-averaged charge recombination time constant (τ_{CR}) of 0.73 μs.

### Global analysis to obtain charge transfer time constants

Although the large energetic separation between SWCNT and MoS_2 spectral features allows us to easily track the recombination lifetimes of separated charges, it is non-trivial to extract accurate rise times for ultrafast charge separation due to the overlapping spectra of excitons and charges at early times. To quantify charge transfer kinetics, we separate the time-dependent spectral contributions of excitons and charges using a global analysis based on singular value decomposition (SVD).[54] We discuss our fitting using TA data for hole transfer following 440 nm excitation (Fig. 4), and we provide fitting results for the

neat materials as well as the heterojunction with 1000 nm excitation in the ESI.†

The SVD analysis expresses the total TA signal $\Psi_{Total}(\lambda,t)$ as a sum of wavelength-dependent spectral signatures $\sigma_i(\lambda)$ with time-dependent concentrations $C_i(t)$, where i denotes the correlation of a spectral signature with an associated population (e.g. excitons on SWCNTs). Since the heterojunction spectra contain only SWCNT features in the NIR range, we analyse the charge-transfer time by separating the spectral contributions of SWCNT singlet excitons and SWCNT charges as $\Psi_{Total}(\lambda,t) = C_{singlet}(t)\sigma_{singlet}(\lambda) + C_{charge}(t)\sigma_{charge}(\lambda)$. Fig. 4 shows an example of our TA fitting results.

Fig. 4A shows the NIR TA spectrum at a pump–probe delay of 1 ps overlaid with the species-associated components that make up the total fit to the data as $\Psi_{Total}(\lambda) = C_{singlet}(1\ ps)\sigma_{singlet}(\lambda) + C_{charge}(1\ ps)\sigma_{charge}(\lambda)$. Even at this early delay, the NIR spectrum for the heterojunction is dominated by charge-associated spectral features with a weaker contribution from SWCNT singlet excitons. We attribute the majority of the charge-associated signal to charge transfer from the MoS_2, although some charge generation may also arise from SWCNT exciton separation following a small amount of off-resonance absorption by the SWCNT layer at 440 nm.

Fig. 4B shows kinetics corresponding to species-associated spectral components of Fig. 4A. We overlay the kinetics data at the peak of the SWCNT trion induced absorption with the fit as $\Psi_{Total}(t) = C_{singlet}(t)\sigma_{singlet}(1175\ nm) + C_{charge}(t)\sigma_{charge}(1175\ nm)$. The $C_{singlet}(t)$ and $C_{charge}(t)$ contributions allow us to separately evaluate the rise and decay of charge carriers (green trace) and

A) Species-Associated Spectra (1 ps)

B) Fitted Kinetics (1175 nm)

C) Electron Transfer vs. Hole Transfer Kinetics
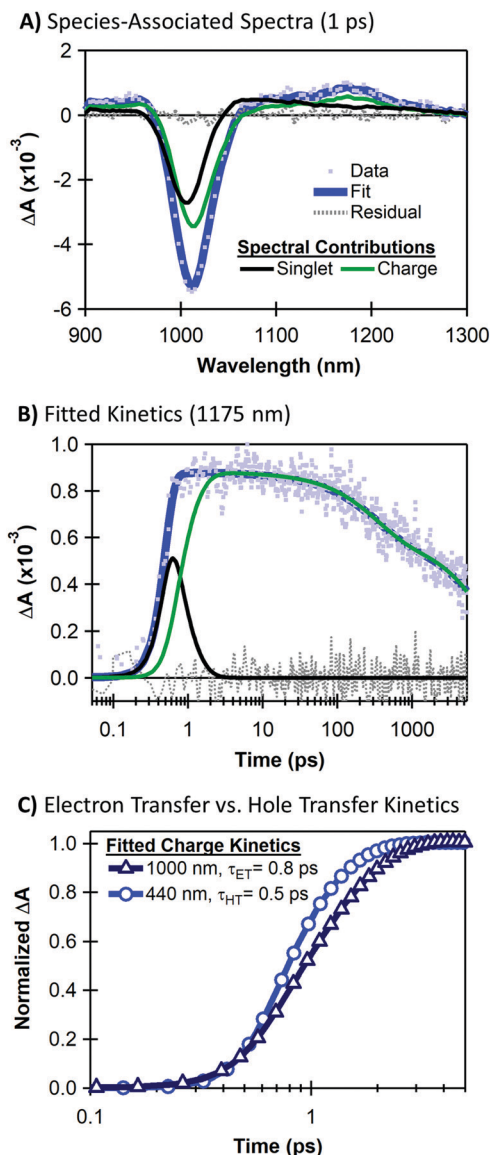
Fig. 4 Example of NIR fitting results for the monolayer MoS_2/SWCNT heterojunction with 440 nm pump including (A) the transient absorption spectrum at 1 ps (light blue points) overlaid with the singlet-associated (black trace) and charge-associated (green trace) spectral components, which are summed to create the total fit (blue trace) giving minimal residual fitting error (gray dotted trace); (B) kinetics at 1175 nm (light blue points) overlaid with the time-dependent profiles corresponding to the spectral components in (A) which are summed to create the total fit (blue trace) giving minimal residual error (gray dotted trace); (C) comparison of the charge-associated kinetics fits showing faster rise for the 440 nm excitation (τ_{HT} = 0.5 ps, blue circles) compared to the 1000 nm excitation (τ_{ET} = 0.8 ps, dark blue triangles) in the heterojunction.

the singlet exciton decay (black trace). We extract a rise time of 0.5 ps for the SWCNT charge signature, corresponding to the hole transfer time from MoS_2 to SWCNTs. The SVD analysis requires three exponential components for the decay of the charge-related spectral signature (further discussed in the ESI†).

Using corresponding fits for the heterojunction TA with selective SWCNT excitation (see Fig. S2, ESI†), Fig. 4C compares the time scales for electron transfer *versus* hole transfer.

Interestingly, we observe slightly faster hole transfer upon selective MoS_2 excitation at 440 nm ($\tau_{ET} \approx$ 0.5 ps) compared to electron transfer following selective SWCNT excitation at 1000 nm ($\tau_{ET} \approx$ 0.8 ps). The faster rise time upon selective MoS_2 excitation may be related to the greater thermodynamic driving force for the hole transfer process (see Fig. 1, $\Delta G_{HT} =$ −620 meV), although it is also possible that this large driving force could place the hole transfer process in the Marcus-inverted regime.[51]

Based on our combined TA analyses, we outline the relevant kinetic processes in Fig. 5, including sub-picosecond charge separation at the monolayer MoS_2/SWCNT interface, where hole transfer proceeds more quickly than electron transfer, followed by very long carrier lifetimes on the 0.73 μs time scale.

Charge transfer quantum yield

Quantifying and optimizing charge transfer yield (ϕ_{CT}) is crucial for targeted design of interfaces supporting high quantum efficiencies for charge separation. ϕ_{CT} is defined as the number of separated charges (N_e or N_h) produced per photogenerated exciton (N_x, taken as the number of absorbed photons). For example, the electron transfer yield is $\phi_{ET} = \dfrac{N_e}{N_x}$. We estimate charge transfer yields for the Type-II MoS_2/SWCNT heterojunctions using two separate methods. One method utilizes an empirically-determined absorption cross section of the (6,5)SWCNT trion induced absorption,[50] which in turn is based on the carrier density dependence of the S_{11} bleaching intensity proposed by Mouri and Matsuda.[59] The other method is based on the expected MoS_2 exciton bleaching in the presence of charge carriers according to a phase-space filling model for quantum-confined excitons in two-dimensional semiconductors.[4]

For the first method, we use the intensity of the trion induced absorption relative to the ground-state S_{11} absorption to estimate $\phi_{ET} \approx$ 23% following selective SWCNT excitation at 1000 nm.[50] In the case of hole transfer, we consider both the fraction of 440 nm light absorbed by MoS_2 and the much smaller fraction of light absorbed by SWCNTs. We estimate $\phi_{HT} \approx$ 39%, assuming that both hole transfer and electron transfer proceed concomitantly, and the small amount of SWCNT excitons that undergo electron transfer to MoS_2 dissociate with the same 23% yield that we observe under 1000 nm excitation. The 39% hole-transfer yield corresponds to 94% of the N_h hole density originating from MoS_2 excitations while SWCNT exciton dissociation accounts for the remaining 6%. We provide fits of the SWCNT trion induced absorption and further discussion of this method for estimating charge-transfer yield in the ESI.†

We further investigate a fully independent method for estimating the hole transfer quantum yield based on a phase-space filling model derived from the 2D exciton Schrödinger equation,[4] which we apply to the MoS_2 bleach amplitude. This method models carrier-induced exciton bleaching using the Pauli exclusion principle, where excess electrons occupying the MoS_2 conduction band (*e.g.* those from charge transfer) block additional transitions from the ground state, thereby decreasing exciton oscillator strength. By representing the exciton
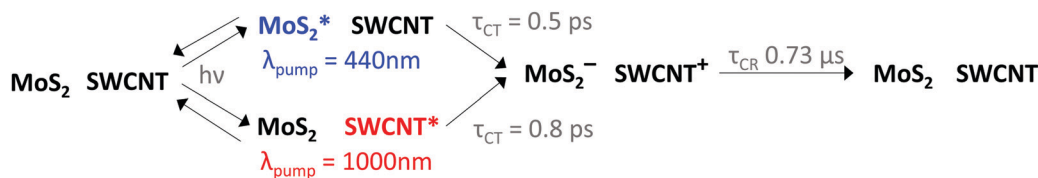
Fig. 5 Kinetic scheme highlighting the different time constants for hole transfer (τ_{HT}) *versus* electron transfer (τ_{ET}) resulting from either selective MoS_2 or SWCNT excitation using pump wavelengths (λ_{pump}) of 440 and 1000 nm, as well as the time constant for charge recombination (τ_{CR}) from the amplitude-averaged lifetime of a triexponential fit.

as an isolated state in an ideal quantum well and assuming its wavefunction is minimally affected by carrier density, a known solution to the Schrödinger equation can be used and the magnitude of exciton bleaching can be related to physical MoS_2 properties such as the dielectric constant (ε), reduced exciton mass (μ), and effective Bohr radius (a_0).[4]

The phase-space filling model gives the fractional decrease in exciton oscillator strength (f) due to a density of N charge carriers as[4]

$$\frac{f(N)}{f(0)} = \frac{1}{1 + N/N_c}. \tag{1}$$

N_c is the critical carrier density at which 50% of the oscillator strength is quenched, which depends on the exciton size as $N_c = 2/\pi a_0^2$, where

$$a_0 = \frac{\varepsilon \hbar^2}{e^2 \mu}, \tag{2}$$

and $\hbar$ is the reduced Planck constant and e is elementary charge.

We estimate the magnitude of carrier-induced bleaching for the MoS_2 A exciton transition (660 nm) at the time when charge transfer is complete and all ground state beaching should be due to the presence of charge carriers. We use the MoS_2-associated spectral components from global target analysis of the heterojunction following 440 nm excitation, which are shown in Fig. 6A. We provide additional discussion of these species-associated spectral shapes and their kinetics in the ESI.† In brief, we associate the earliest component with decay of the initial singlet population with a 0.9 ps time constant, and we associate the longer-lived components with charge carriers (31 ps and >5 ns decay constants). We estimate charge-induced bleaching by the amplitude of the 660 nm bleach when the initial charge-associated component reaches its maximum concentration ($\sim$3.5 ps). We evaluate $f(N)/f(0)$ using the ground-state absorption A and transient absorption ΔA from Fig. 6A as $(A - \Delta A)/A = 0.94$. In Fig. 6B, we demonstrate the intersection between this magnitude of exciton bleaching that we observe in the TA data with the phase-space filling model.

Importantly, eqn (1) and (2) show that the magnitude of carrier-induced exciton bleaching depends on the dielectric constant and the exciton mass, which influence the exciton size in opposite ways. For Fig. 6B, we use an average reduced exciton mass from the literature of $0.25m_e$ (where m_e is the electron mass),[33,34,60–63] and we display multiple plots with dielectric constants ranging from 4–30.[5,63–66] The horizontal line in Fig. 6B represents the magnitude of carrier-induced exciton

Fig. 6 (A) Species-associated components for an MoS_2/SWCNT heterojunction under 440 nm excitation from global target analysis using a sequential model with decay time constants given for each component; (B) charge density (N) dependence of the exciton oscillator strength (f) from a phase-space filling model described in ref. 4, plotted for varying dielectric constants and overlaid with a horizontal line at the exciton quenching value from transient absorption analysis ($f(N)/f(0) = 0.94$). The rainbow section spans carrier densities corresponding to charge-transfer quantum yields of red = 10% to purple = 100%. The green $f(N)/f(0)$ trace corresponds to a 39% charge-transfer yield.

bleaching that we observe in our TA data of $f(N)/f(0) = 0.94$. We highlight a region of this horizontal line with a rainbow gradient indicating the range of possible photogenerated carrier densities with red at 10% charge-transfer quantum yield and purple at 100%. The 10–100% range intersects the $f(N)/f(0)$ traces with dielectric constants of $\varepsilon = 19$ (for 10% yield) and $\varepsilon = 8$ (for 100% yield). The green curve highlights 39% charge-transfer quantum yield (corresponding to $\varepsilon = 10$ and $a_0 = 2.2$ nm), matching our estimate of hole-transfer yield from the SWCNT trion induced absorption.

We note that determining an appropriate value for the dielectric constant experienced by an exciton in monolayer MoS_2 is not trivial,[5,64–66] and the trends in Fig. 6B highlight its significant impact on the magnitude of carrier-induced exciton bleaching. The dielectric constant of monolayer MoS_2 has been the topic of many theoretical and experimental investigations, and values vary considerably depending on MoS_2 thickness, sample plane, substrate, defects, and growth methods.[5,64–66] Indeed, literature values of MoS_2 monolayer dielectric constants[5,63–66] vary much more substantially compared to values for exciton mass.[33,34,60–63] Importantly, Fig. 6B shows that our observed exciton bleaching from TA measurements does intersect the phase-space filling model at realistic charge-transfer quantum yields with reasonable MoS_2 materials parameters, though the uncertainty in the dielectric constant prevents us from confidently extracting a value for charge-transfer quantum yield from this model. Further evaluation of the phase-space filling model and its applicability to monolayer TMDCs could enable this as a new method for using optical signatures to compare dielectric environments across different TMDCs or fabrication methods. In general, accurately estimating charge transfer yield for nanoscale heterojunctions such as these is non-trivial and should be the subject of continued investigation and refinement.

Conclusions

The 0.5 ps hole-transfer time constant (τ_{HT}) that we observe at the monolayer MoS_2/SWCNT interfaces is on par with or even faster than recently-reported time constants for hole transfer in organic/MoS_2 heterojunctions, including pentacene/MoS_2 with $\tau_{HT} \approx 6.7$ ps[44] and polymer (PTB7)/MoS_2 with $\tau_{HT} \approx 1–5$ ps.[42] In addition to this faster hole transfer time, an important advantage of SWCNT/MoS_2 heterojunction systems over polymer or small molecule heterojunctions is the exceptional chemical and photo-stability of the SWCNTs, implying that this type of heterojunction is a truly viable option for photocatalytic systems where photons can drive hydrogen evolution in aqueous environments at low pH (high proton concentrations). While TMDC/TMDC heterojunctions may promise even faster hole transfer times, it is important to note that charge transfer in these systems is characterized by the formation of tightly bound interfacial excitons that decay rapidly on picosecond time scales, as carriers are spatially confined and have limited ability to move away from the interface.[37]

The 0.8 ps electron-transfer time (τ_{ET}) for the monolayer MoS_2/SWCNT system is slightly slower than that at TMDC/TMDC and other MoS_2/organic heterojunctions. We attribute the slower τ_{ET} to the low driving force for SWCNT exciton separation and subsequent charge transfer to monolayer MoS_2. With sufficient driving force, interfacial electron transfer following SWCNT exciton dissociation can occur on faster time scales (<120 fs) and with correspondingly higher yields.[50] In the current model system, we suspect that the charge-transfer yield could be optimized through many avenues such as (1) increasing the driving force and carrier delocalization either by using

nanotubes with different diameters or TMDCs with higher electron affinity; (2) exploring the effect of TMDC defect density, lateral continuity, layer number, and internal strain on charge transfer kinetics and yield; (3) increasing the thickness of the SWCNT layer to support longer range charge separation; (4) tuning the effective MoS_2 dielectric constant; or (5) altering the SWCNT/TMDC interface by doping of either or both semiconductor.

Optimizing the charge-transfer yield, in conjunction with maintaining or increasing the already exceptionally long 0.73 μs carrier lifetimes, could enable efficient photocurrent generation and hydrogen evolution devices employing these interfaces. Importantly, the 0.73 μs lifetime of charge-separated states in the MoS_2/SWCNT heterojunctions is to our knowledge orders of magnitude longer than lifetimes for charge-separated states in other TMDC systems.[42,44] To a large extent, we credit the long lifetime to the excellent ability of the SWCNT layer to sustain and delocalize charge, allowing carriers to efficiently move away from the MoS_2 interface. Indeed, organic heterojunctions employing SWCNT films have also achieved lifetimes exceeding 1 μs.[14] It is also possible that the SWCNT layer helps to decrease carrier trapping by passivating MoS_2 surface defects, as has previously been proposed for other organic/TMDC interfaces.[67]

Our study demonstrates the promise of pairing TMDCs with SWCNTs both for enabling functional applications requiring ultrafast charge generation and exceptionally long-lived carriers as well as for use as a clean model system for optical studies of TMDCs based on well-characterized and clearly resolvable SWCNT spectral signatures. Future studies of TMDC/SWCNT heterojunctions should probe the roles of both in-plane and out-of-plane carrier delocalization and/or diffusion in stabilizing long-lived charges. The well-defined SWCNT charge-associated signatures should also be useful for probing the roles of thermodynamic driving force and dielectric environment on charge separation and recombination in a variety of TMDCs.

Conflicts of interest

There are no conflicts to declare.

Acknowledgements

References

1 H. Li, C. Tsai, A. L. Koh, L. Cai, A. W. Contryman, A. H. Fragapane, J. Zhao, H. S. Han, H. C. Manoharan, F. Abild-Pedersen, J. K. Nørskov and X. Zheng, *Nat. Mater.*, 2015, **15**, 48.

2 H. Huang, W. Huang, Z. Yang, J. Huang, J. Lin, W. Liu and Y. Liu, *J. Mater. Chem. A*, 2017, **5**, 1558.

3 X. Han, X. Tong, X. Liu, A. Chen, X. Wen, N. Yang and X.-Y. Guo, *ACS Catal.*, 2018, **8**, 1828.

4 D. Huang, J.-I. Chyi and H. Morkoç, *Phys. Rev. B: Condens. Matter Mater. Phys.*, 1990, **42**, 5147.

5 S. Park, N. Mutz, T. Schultz, S. Blumstengel, A. Han, A. Aljarb, L.-J. Li, E. J. W. List-Kratochvil, P. Amsalem and N. Koch, *2D Mater.*, 2018, **5**, 025003.

6 F. Davoodi and N. Granpayeh, *Opt. Quantum Electron.*, 2018, **51**, 9.

7 B. Radisavljevic, A. Radenovic, J. Brivio, V. Giacometti and A. Kis, *Nat. Nanotechnol.*, 2011, **6**, 147.

8 H. Wang, L. Yu, Y.-H. Lee, Y. Shi, A. Hsu, M. L. Chin, L.-J. Li, M. Dubey, J. Kong and T. Palacios, *Nano Lett.*, 2012, **12**, 4674.

9 Y. Liu, J. Guo, E. Zhu, L. Liao, S.-J. Lee, M. Ding, I. Shakir, V. Gambin, Y. Huang and X. Duan, *Nature*, 2018, **557**, 696.

10 M. Bernardi, M. Palummo and J. C. Grossman, *Nano Lett.*, 2013, **13**, 3664.

11 Y. Zhang, H. Yu, R. Zhang, G. Zhao, H. Zhang, Y. Chen, L. Mei, M. Tonelli and J. Wang, *Opt. Lett.*, 2017, **42**, 547.

12 T. A. Shastry, I. Balla, H. Bergeron, S. H. Amsterdam, T. J. Marks and M. C. Hersam, *ACS Nano*, 2016, **10**, 10573.

13 J. Wong, D. Jariwala, G. Tagliabue, K. Tat, A. R. Davoyan, M. C. Sherrott and H. A. Atwater, *ACS Nano*, 2017, **11**, 7230.

14 H. S. Kang, T. J. Sisto, S. Peurifoy, D. H. Arias, B. Zhang, C. Nuckolls and J. L. Blackburn, *J. Phys. Chem. C*, 2018, **122**, 14150.

15 R. G. Dickinson and L. Pauling, *J. Am. Chem. Soc.*, 1923, **45**, 1466.

16 P. Joensen, R. F. Frindt and S. R. Morrison, *Mater. Res. Bull.*, 1986, **21**, 457.

17 M. J. Allen, V. C. Tung and R. B. Kaner, *Chem. Rev.*, 2010, **110**, 132.

18 S. Manzeli, D. Ovchinnikov, D. Pasquier, O. V. Yazyev and A. Kis, *Nat. Rev. Mater.*, 2017, **2**, 17033.

19 W. Choi, N. Choudhary, G. H. Han, J. Park, D. Akinwande and Y. H. Lee, *Mater. Today*, 2017, **20**, 116.

20 A. Splendiani, L. Sun, Y. Zhang, T. Li, J. Kim, C.-Y. Chim, G. Galli and F. Wang, *Nano Lett.*, 2010, **10**, 1271.

21 K. F. Mak, C. Lee, J. Hone, J. Shan and T. F. Heinz, *Phys. Rev. Lett.*, 2010, **105**, 136805.

22 S. Pak, J. Lee, Y.-W. Lee, A. R. Jang, S. Ahn, K. Y. Ma, Y. Cho, J. Hong, S. Lee, H. Y. Jeong, H. Im, H. S. Shin, S. M. Morris, S. Cha, J. I. Sohn and J. M. Kim, *Nano Lett.*, 2017, **17**, 5634.

23 Y. Sun and K. Liu, *J. Appl. Phys.*, 2018, **125**, 082402.

24 H. Nan, Z. Wang, W. Wang, Z. Liang, Y. Lu, Q. Chen, D. He, P. Tan, F. Miao, X. Wang, J. Wang and Z. Ni, *ACS Nano*, 2014, **8**, 5738.

25 S. Mouri, Y. Miyauchi and K. Matsuda, *Nano Lett.*, 2013, **13**, 5944.

26 X. Xu, W. Yao, D. Xiao and T. F. Heinz, *Nat. Phys.*, 2014, **10**, 343.

27 D. Xiao, G.-B. Liu, W. Feng, X. Xu and W. Yao, *Phys. Rev. Lett.*, 2012, **108**, 196802.

28 Z.-Z. Zhang, X.-X. Song, G. Luo, G.-W. Deng, V. Mosallanejad, T. Taniguchi, K. Watanabe, H.-O. Li, G. Cao, G.-C. Guo, F. Nori and G.-P. Guo, *Sci. Adv.*, 2017, **3**, e1701699.

29 J. G. Roch, N. Leisgang, G. Froehlicher, P. Makk, K. Watanabe, T. Taniguchi, C. Schönenberger and R. J. Warburton, *Nano Lett.*, 2018, **18**, 1070.

30 M. N. Ali, J. Xiong, S. Flynn, J. Tao, Q. D. Gibson, L. M. Schoop, T. Liang, N. Haldolaarachchige, M. Hirschberger, N. P. Ong and R. J. Cava, *Nature*, 2014, **514**, 205.

31 D. Kang, Y. Zhou, W. Yi, C. Yang, J. Guo, Y. Shi, S. Zhang, Z. Wang, C. Zhang, S. Jiang, A. Li, K. Yang, Q. Wu, G. Zhang, L. Sun and Z. Zhao, *Nat. Commun.*, 2015, **6**, 7804.

32 M. Khezerlou and H. Goudarzi, *Phys. Rev. B*, 2016, **93**, 115406.

33 S. Latini, K. T. Winther, T. Olsen and K. S. Thygesen, *Nano Lett.*, 2017, **17**, 938.

34 A. Thilagam, *J. Appl. Phys.*, 2014, **116**, 053523.

35 D. Vella, D. Ovchinnikov, D. Viola, D. Dumcenco, Y. C. Kung, E. A. A. Pogna, S. D. Conte, V. Vega-Mayoral, T. Borzda, M. Prijatelj, D. Mihailovic, A. Kis, G. Cerullo and C. Gadermaier, *2D Mater.*, 2017, **4**, 035017.

36 D. Vikraman, S. Hussain, K. Akbar, L. Truong, A. Kathalingam, S.-H. Chun, J. Jung, H. J. Park and H.-S. Kim, *ACS Sustainable Chem. Eng.*, 2018, **6**, 8400.

37 X. Hong, J. Kim, S.-F. Shi, Y. Zhang, C. Jin, Y. Sun, S. Tongay, J. Wu, Y. Zhang and F. Wang, *Nat. Nanotechnol.*, 2014, **9**, 682.

38 M. Tosun, D. Fu, S. B. Desai, C. Ko, J. Seuk Kang, D.-H. Lien, M. Najmzadeh, S. Tongay, J. Wu and A. Javey, *Sci. Rep.*, 2015, **5**, 10990.

39 S. L. Howell, D. Jariwala, C.-C. Wu, K.-S. Chen, V. K. Sangwan, J. Kang, T. J. Marks, M. C. Hersam and L. J. Lauhon, *Nano Lett.*, 2015, **15**, 2278.

40 Y. Yang, N. Huo and J. Li, *J. Mater. Chem. C*, 2017, **5**, 7051.

41 T. R. Kafle, B. Kattel, S. D. Lane, T. Wang, H. Zhao and W.-L. Chan, *ACS Nano*, 2017, **11**, 10184.

42 C. Zhong, V. K. Sangwan, C. Wang, H. Bergeron, M. C. Hersam and E. A. Weiss, *J. Phys. Chem. Lett.*, 2018, **9**, 2484.

43 Y. L. Huang, Y. J. Zheng, Z. Song, D. Chi, A. T. S. Wee and S. Y. Quek, *Chem. Soc. Rev.*, 2018, **47**, 3241.

44 S. Bettis Homan, V. K. Sangwan, I. Balla, H. Bergeron, E. A. Weiss and M. C. Hersam, *Nano Lett.*, 2017, **17**, 164.

45 T. Guo, S. Sampat, K. Zhang, J. A. Robinson, S. M. Rupich, Y. J. Chabal, Y. N. Gartstein and A. V. Malko, *Sci. Rep.*, 2017, **7**, 41967.

46 M.-L. Tsai, S.-H. Su, J.-K. Chang, D.-S. Tsai, C.-H. Chen, C.-I. Wu, L.-J. Li, L.-J. Chen and J.-H. He, *ACS Nano*, 2014, **8**, 8317.

47 X. Qian, J. Ding, J. Zhang, Y. Zhang, Y. Wang, E. Kan, X. Wang and J. Zhu, *Nanoscale*, 2018, **10**, 1766.

48 Z. Zhang, W.-Q. Huang, Z. Xie, W. Hu, P. Peng and G.-F. Huang, *J. Phys. Chem. C*, 2017, **121**, 21921.

49 P. Li, Z. Yang, J. Shen, H. Nie, Q. Cai, L. Li, M. Ge, C. Gu, X. A. Chen, K. Yang, L. Zhang, Y. Chen and S. Huang, *ACS Appl. Mater. Interfaces*, 2016, **8**, 3543.

50 A.-M. Dowgiallo, K. S. Mistry, J. C. Johnson and J. L. Blackburn, *ACS Nano*, 2014, **8**, 8573.

51 R. Ihly, K. S. Mistry, A. J. Ferguson, T. T. Clikeman, B. W. Larson, O. Reid, O. V. Boltalina, S. H. Strauss, G. Rumbles and J. L. Blackburn, *Nat. Chem.*, 2016, **8**, 603.

52 W. Rui, W. Tianjiao, H. Tu and X. Ya-Qiong, *Nanotechnology*, 2018, **29**, 345205.

53 D. Jariwala, V. K. Sangwan, C.-C. Wu, P. L. Prabhumirashi, M. L. Geier, T. J. Marks, L. J. Lauhon and M. C. Hersam, *Proc. Natl. Acad. Sci. U. S. A.*, 2013, **110**, 18076.

54 J. J. Snellenburg, S. Laptenok, R. Seger, K. M. Mullen and I. H. M. van Stokkum, *J. Stat. Softw.*, 2012, **49**, 1.

55 M. Zdrojek, T. Mélin, H. Diesinger, D. Stiévenard, W. Gebicki and L. Adamowicz, *J. Appl. Phys.*, 2006, **100**, 114326.

56 T. Dürkop, S. Getty, E. Cobas and M. Fuhrer, *Nano Lett.*, 2004, **4**, 35.

57 D. C. Coffey, B. W. Larson, A. W. Hains, J. B. Whitaker, N. Kopidakis, O. V. Boltalina, S. H. Strauss and G. Rumbles, *J. Phys. Chem. C*, 2012, **116**, 8916.

58 Y. Yu, C. Li, Y. Liu, L. Su, Y. Zhang and L. Cao, *Sci. Rep.*, 2013, **3**, 1866.

59 S. Mouri and K. Matsuda, *J. Appl. Phys.*, 2012, **111**, 094309.

60 A. Ramasubramaniam, *Phys. Rev. B: Condens. Matter Mater. Phys.*, 2012, **86**, 115409.

61 F. A. Rasmussen and K. S. Thygesen, *J. Phys. Chem. C*, 2015, **119**, 13169.

62 T. C. Berkelbach, M. S. Hybertsen and D. R. Reichman, *Phys. Rev. B: Condens. Matter Mater. Phys.*, 2013, **88**, 045318.

63 Y. Yu, Y. Yu, Y. Cai, W. Li, A. Gurarslan, H. Peelaers, D. E. Aspnes, C. G. Van de Walle, N. V. Nguyen, Y.-W. Zhang and L. Cao, *Sci. Rep.*, 2015, **5**, 16996.

64 S.-L. Li, K. Tsukagoshi, E. Orgiu and P. Samorì, *Chem. Soc. Rev.*, 2016, **45**, 118.

65 A. Laturia, M. L. Van de Put and W. G. Vandenberghe, *npj 2D Mater. Appl.*, 2018, **2**, 6.

66 E. J. G. Santos and E. Kaxiras, *ACS Nano*, 2013, **7**, 10741.

67 J. H. Park, A. Sanne, Y. Guo, M. Amani, K. Zhang, H. C. P. Movva, J. A. Robinson, A. Javey, J. Robertson, S. K. Banerjee and A. C. Kummel, *Sci. Adv.*, 2017, **3**, e1701661.